Nanoscale

Accepted Manuscript

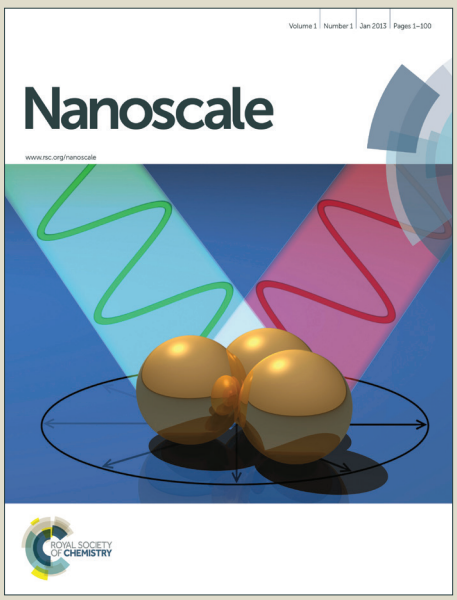

ROYAL SOCIETY OF CHEMISTRY

www.rsc.org/nanoscale

Na^+ and K^+ ion selectivity by size-controlled biomimetic graphene nanopores

Yu Kang[1, §], Zhisen Zhang[1, §], Hui Shi[1], Junqiao Zhang[1], Lijun Liang[1,2,*], Qi Wang[1,*], Hans Ågren[2], Yaoquan Tu[2]

[1]Department of Chemistry and Soft Matter Research Center, Zhejiang University, Hangzhou 310027, People's Republic of China

[2]Division of Theoretical Chemistry and Biology, School of Biotechnology, KTH Royal Institute of Technology, SE-10691 Stockholm, Sweden

*Corresponding authors.

Fax: +86-571-87951895.

E-mail addresses:

qiwang@zju.edu.cn (Q. Wang)

michael.lijunl@gmail.com (Lijun Liang)

§: these authors contributed equally to this work

Abstract

Owing to that biological ionic channels play a key role in cellular transport phenomena they have attracted intense research interest for the design of biomimetic nanopores with high permeability and selectivity for a variety of technical applications. Inspired by the structure of K^+ channel proteins, we design by molecular dynamics simulations a series of oxygen doped graphene nanopores of different size to discriminate between K^+ and Na^+ channel transport. The results from free energy calculations indicate that the ion selectivity of such biomimetic graphene nanopores can be simply controlled by the size of the nanopore - compared to K^+, the smaller radius of Na^+ leads to a much higher free energy barrier in the nanopore of a certain size. Our results suggest that graphene nanopores with the distance of about 3.9 Å between two neighboring oxygen atoms could constitute a promising candidate to obtain excellent ion selectivity for Na^+ and K^+ ions.

1. Introduction

Ionic channels in proteins play a key role in many cellular transport phenomena[1] and provide sources of inspiration for the development of a variety of biomimetic type of nanopores. This notion is based on the fact that biological ionic channels contain precisely arranged charged amino acids to achieve extremely high permeability simultaneously with high selectivity to pass the ions[2]. These superior selectivity features of biological channels have attracted much research interest [3]and inspired many experiments and theoretical studies alike to mimic these properties in technical applications[4-10]. Proteins can always lose their bioactivity without the biological setting [11]and harsh environmental demands and poor mechanical properties of proteins have strictly limited their applications ex-vivo. Therefore, it would be of great value if the key functionalized core of proteins could be simulated by man-made mechanical nanopores to be used in industrial applications. The simulation of functions of proteins is also very important to the development of biomimetic materials in general.

Solid state nanopores fabricated from graphene sheets[12-14] have attracted much attention due to the unique properties of graphene[15, 16]. Thanks to the fast development of etching nanotechnology, graphene nanopores with radii as small as 0.3nm have been synthesized[17]. Many studies have shown that graphene nanopores can be used in functionalized applications[13, 14, 18-25]. Jiang et al. found that graphene nanopores can be used for gas separation[20]; Aksimentiev et al. used molecular dynamics (MD) simulations to show that graphene nanopores can be used for DNA sequencing[23]; Sint et al. demonstrated the selectivity of ion passage by means of functionalized graphene nanopores[24]; and Zeng et al. reported an outstanding graphyne membrane for water desalination at high rate and potentially low cost[25].

Thus, graphene is a promising biomimetic material for a variety of applications, such as for nanofluidics, biosensors, and for ion selectivity devices.

To mimic the functions of proteins, it is essential to understand their core structures and functional mechanisms. Herein, the potassium channel from streptomyces lividans (KcsA) (PDB ID: 1BL8) was selected as a model protein[26]. As we know, the properties of Na^+ and K^+ are almost the same since they are both alkali cations with the same charge; thus, it is difficult to distinguish them by simple pores like those in zeoiltes [27] and silica[28]. However, biological K^+ channels have the ability to make an up to 1000-fold selection of K^+ from Na^+[29]. The functional core in K^+ channel proteins is an ion filter which is lined up by four rings of backbone carbonyl groups which compensate the lost energy during the dehydration process.

In this work, graphene nanopores with different radii are designed for ion selectivity for Na^+ and K^+ by means of MD simulations. We study the sensitivity and the separability of Na^+ and K^+ ions with respect to the variation of pore dimensions in order to disclose the optimal conditions, attempting to find a deeper explanation for selectivity in this respect. The work can be seen as a step towards rational design of graphene nanopores for practical applications.

2. Simulation methods

2.1 Conformation optimization of the nanopores by first-principle methods

To obtain reasonable configurations of the graphene nanopores, density-functional-theory (DFT) calculations were performed with the Vienna *ab initio* simulation package[30, 31]. Projector-augmented wave potential and generalized gradient approximation, in the form of Perdew-Burke-Ernzerhof functional were adopted[32]. The valence wave functions were

expanded in a plane-wave basis with a cutoff energy of 500 eV, with O 1s and C 1s electrons treated as core states. A vacuum width of 15 Å was chosen for the structure optimization. All atoms were allowed to relax. The geometry was converged until the force acting on each atom was less than 0.02 eV/Å, and a Monkhorst-Pack grid of 5×5×1 was used[33]. The outcome of this initial conformation optimization was used in the subsequent MD simulations. According to the results of the first-principle calculations, the C atoms and O atoms are coplanar - the detail of conformation is seen in Fig.1.

2.2 System build-up

Three kinds of graphene nanopores with different size were constructed according to the structure of the potassium channel in KcsA (as seen in Fig. 1). The conformations of the nanopores were optimized by first-principle calculations and all graphene atoms were fixed in the following MD simulations. Simulations with free graphene nanopores were also performed for comparison to check how the flexibility of the oxygen doped graphene may affect the results (see Supporting Information). The geometry of the simulation box is shown in Fig. 2. To construct a system, a graphene sheet was placed at the left edge of the simulation box as a wall, and a graphene nanopore was placed in the simulation box, dividing the whole system into two independent parts named as the left "area A" and the right "area B". The nanopore is the only way for ions to move from area A to area B. For each system, the graphene sheet and ions were placed in a box with size of 3.83×3.95×6.00 nm^3 and solvated by ~2700 TIP3P water molecules to reach a density of ~1.00 g/m^3. After the energy minimization, the system was equilibrated in the NPT ensemble for 10 ns, in prior to the production run.

2.3 MD simulation details

All the production runs of the MD simulation in this work are performed in the NVT ensemble using the Gromacs 4.2.5 package[34, 35]. The visualization was generated via visual molecular dynamics (VMD) [36]. Periodic boundary condition was applied to all of the three directions. All bonds that involve H-atoms were fixed. A time step of 2 fs was used with atom coordinates saved every 2 ps. A temperature of 298 K was maintained using the V-rescale method, and the TIP3P water model was applied to the solvent water molecules[37]. The CHARMM27 all-atom force field was used for describing the ions[38]. The parameters of graphene were obtained from our previous work[39, 40], and the parameters of the O atoms around a nanopore were assumed to be the same as those for the O atom in the peptide bond in the CHARMM27 all-atom force field, with the atomic charge = -0.51 |e|, σ = 0.30291 nm, and ε = 0.50208 kJ/mol. The atoms of the graphene remain fixed in all the MD simulations. The particle mesh Ewald (PME) summation [41] was used to calculate the long range electrostatic interaction, with a cutoff of 1.3 nm for the separation of the direct and reciprocal space summation. The cutoff distance for the van der Waals interaction was 1.3 nm; the parameters of the Lennard-Jones potential for the cross interactions between non-bonded atoms were obtained from the venerable Lorentz-Berthelot combination rule[42].

2.4 Ion selectivity under different electric fields

Electric fields were applied to the systems to reveal K^+/Na^+ selectivity of the three kinds of graphene nanopores. At the beginning of the simulation, ten K^+ and ten Na^+ ions were added

only to the "area A" of the system, and Cl^- ions were also added to "area A" to balance the net charge of the system. The system was subsequently equilibrated, and a 10 ns MD simulation was performed. After that, the number of K^+/Na^+ ions in "area B" was extracted to analyze the ion selectivity of the graphene nanopore.

2.5 Density distributions in the *z*-axis direction and radial distribution functions (RDFs)

Unlike the initial configuration in the ion selectivity analysis, ten K^+ and ten Na^+ ions were added into both areas, and Cl^- ions were also added to balance the net charge. Then a 20 ns MD simulation was performed, and the density distributions of K^+/Na^+ ions in the *z*-axis direction were extracted. The RDFs of K^+/Na^+ ions around the O atoms of the graphene nanopore were calculated by using the data from the last 15ns of the simulations.

2.6 Free energy calculations: Umbrella sampling

The free energy profiles (represented by potentials of mean force, PMFs) were calculated by umbrella sampling[43-45]. PMFs were calculated along the reaction coordinate which was defined as the z-component distance between the ions and the center of a graphene nanopore. In principle, the PMFs should be symmetric with respect to the two sides of the graphene nanopore. Thus the umbrella sampling was only performed for the reaction coordinate varied from -1.4 nm to 0.1 nm and the PMF for 0-1.4 nm was generated from that for -1.4-0 nm by the symmetry. The width of umbrella windows was 0.2 nm for the reaction coordinate varied from -1.4 nm to -0.4 nm, and 0.1 nm for -0.4 nm to 0.1 nm to enhance the sampling around the graphene nanopore. A 10 ns simulation was performed for each umbrella window, in which the

K^+ or Na^+ ions were restrained in the *z* direction using a harmonic force with a constant of 1000 kJ · mol^{-1} · nm^{-2}. The first 4 ns in each umbrella simulation was used to reach equilibrium, and the latter 6 ns were used to generate the final PMFs via the weighted histogram analysis method[46].

3. Results and discussion

3.1 Biomimetic graphene nanopores

The main constituents of the ion-selectivity filter of the K^+ channel protein KcsA are the main-chain carbonyl oxygen atoms that form a series of stereochemical circles. Each circle consists of four oxygen atoms that surround K^+ ions as they pass through the circle. The distance between neighboring O atoms in each circle is different (Fig. 1a), which could stabilize the dehydrated K^+. To well reproduce the function of the K^+ channel, one of the most important tasks is to place the O atoms with proper intervals. For example, nanopore II (Fig. 1b, Fig. 3a) was set up to mimic the filter core with the O-O distance of 3.89 Å. In order to first unravel the chemical effect of the O atoms, a nanopore with the same geometry as nanopore II but with all the O atoms replaced with C atoms is used for comparison (denoted as nanopore IV as shown in Fig. 3b). The density distributions of K^+/Na^+ ions along the *z*-axis of the nanopores II and IV are shown in Fig. 3. In nanopore IV, there are two major peaks for both Na^+ and K^+ residing on each side of the nanopore. The first peak is at 4.94 Å from the center of the nanopore for Na^+ and 5.95 Å for K^+, respectively. During a 10-ns simulation no ions were observed passing through nanopore IV corresponding to that the density is zero at z=0. In the case of nanopore II, however, there is one more peak in the density profile which is located quite close to the

nanopore (d = 1.46 Å for Na^+ and d = 2.58 Å for K^+). What is more important is that in the K^+ case one peak at d = 0 Å can be found, corresponding to the K^+ permeation through the nanopore. This proves that the extra peaks in the density profiles of nanopore II are due to the existence of the O atoms with strong electrostatic attractions to the cations, which makes the cations gather in the vicinity of the nanopore II. Moreover, the local maximum of the density distribution in the nanopore II (z=0 Å) can only be found for K^+ but not for Na^+. This indicates that it is easier for K^+ to pass through the nanopore II, while Na^+ can hardly pass and just gather in the vicinity instead, meaning that nanopore II preferentially allows the K^+ ions to get through. Here we would like to draw the conclusion that the function of the KcsA K^+ channel has been achieved by the designed nanopore II. It is thus interesting to see that nanopore II can reproduce the function of the ion-selectivity filter by just mimicking the size of the nanopore constructed by the neighboring O atoms.

In the KcsA K^+ channel there are mainly O-atom quaternion rings with three sizes: 3.12/3.33 Å, 3.89 Å and 4.22 Å (Fig. 1a). The size of nanopore II in graphene is similar to the O-atom quaternion ring with a side length of 3.89 Å. Two other nanopores in graphene were then constructed according to the O-atom quaternion rings with side lengths of 3.12/3.33 Å and 4.22 Å in the KcsA K^+ channel, which were named nanopore I (Fig. 1b) and nanopore III (Fig. 1d), respectively. The ion selectivity was further investigated as follows.

3.2 Ion selectivity of graphene nanopores of different size

In order to further mimic the entire ion-selectivity filter of KcsA, MD simulations were carried out for the three designed nanopores I, II, and III with different pore sizes corresponding to the O-atom quaternion rings in KcsA. In a previous work[47], He *et al* pointed out that the ion selectivity could be tuned by an electric field. In this work, we systematically consider the ion permeation influenced by an electric field in combination with the pore size. The number of K^+ and Na^+ ions passing through each kind of nanopores under different applied electric fields was counted as shown in Fig. 4. In the smallest nanopore I, the number of Na^+ and K^+ ions passing through is very small under a low electric field, and increases with the increase of the applied electric field. The ratio of the number of K^+ ions passing through the nanopore to that of Na^+ ions was calculated as Num_{K^+}/Num_{Na^+}. In the case of nanopore I (see Fig.4a), the value of Num_{K^+}/Num_{Na^+} is between 0.5 and 2 for all the applied electric fields. This indicates that the K^+/Na^+ selectivity is small within the range of 200-1000 mV/nm. In the KcsA K^+ channel, the O-atom quaternion ring (with side length of 3.12/3.33 Å) was located in the middle of the filter core; thus, the ion selectivity is not the main function for this nanopore. The ion selectivity of the corresponding graphene nanopore I for the Na^+ and K^+ ions is also not desirable in our simulation. In the middle-sized nanopore II, all values of Num_{K^+}/Num_{Na^+} is over 1.7 for different electric fields, and the highest value is 7 for the applied electric field of 400 mv/nm as seen in Fig.4b and Fig.5. Nanopore II exhibits a remarkable discrimination for Na^+ and K^+, which will be further discussed in the following section. In the KcsA K^+ channel, the O-atom quaternion ring with side length of 3.9 Å was the gate of the filter core which serves as the first checkpoint. The corresponding graphene nanopore II shows the most remarkable ion selectivity. This means that the function of the KcsA K^+ channel has been realized by graphene nanopore II

of the same size, even though the number of the surrounding O-atoms is different. In the largest nanopore III, the value of Num_{K^+}/Num_{Na^+} is over 1.5, and the highest one is 4 under the applied electric field of 600mV/nm as shown in Fig.4c. The ion selectivity for this nanopore is better than for nanopore I but not as good as that of nanopore II. These results suggest that the electric field could tune the ion selectivity only under the condition that the size of the nanopore is in an appropriate range, because the process is primarily controlled by the size of the nanopore. As both the natural ion-selectivity filter and the bio-inspired nanopores have relatively rigid and symmetric structures, the mechanism of the ion selectivity could be simplified as a geometric issue.

Since among the three kinds of the graphene nanopores with different sizes, nanopore II exhibits an outstanding K^+ selectivity over Na^+, a detailed investigation on the size of graphene nanopore II is further carried out in section 3.4. In order to draw a more convincing picture of the K^+ selectivity over Na^+ in nanopore II, one should address the issue of sufficient sampling. Thus, to better understand the mechanism of the ion selectivity of graphene nanopore II, umbrella sampling was employed to calculate the PMF profiles of K^+ and Na^+ ions passing through the nanopore as described in the following section.

3.3 Ion selectivity

Using PMF sampling the quality of K^+/Na^+ selectivity of graphene nanopore II can be quantitatively demonstrated by the difference between the PMF profiles. These profiles are shown in Fig. 6 for K^+/Na^+ passing through nanopore II. The highest free energy barrier for Na^+ passing through the nanopore is 33.6 kJ/mol and is located in the nanopore. This result

indicates that it is very difficult for Na^+ to pass through the nanopore, since the free energy barrier is so large. On the other hand, the highest free energy barrier for K^+ passing through the nanopore is only 12.4 kJ/mol and located at 0.11 nm away from the pore. An interesting aspect here is that the nanopore center is a saddle point in the PMF profile for K^+ passing through the nanopore. This means that the nanopore center is a meta-stable location for K^+. The difference in the free energy barriers for K^+ and Na^+ to pass through the nanopore is about 21 kJ/mol. According to transition state theory, we can estimate the reaction rate constants for K^+ and Na^+, which are expressed by Eq.(1). Since the initial number of K^+ and Na^+ are both 10, the reaction rates for K^+ and Na^+ to pass through nanopore II can be assumed to be proportional to their reaction rate constants. This means that the nanopore's selectivity for K^+ over Na^+ can be estimated by $k(K^+)/k(Na^+)$, where k is the reaction rate constant. The ratio of selectivity so estimated is about 1000:1 which suggests that the K^+ selectivity (over Na^+) of nanopore II could match with that of the natural K^+ channel of the KcsA protein.

$$k\left(\mathrm{Na}^+\right) \propto e^{-\frac{\Delta G\left(\mathrm{Na}^+\right)}{RT}} \quad , \quad k\left(\mathrm{K}^+\right) \propto e^{-\frac{\Delta G\left(\mathrm{K}^+\right)}{RT}} \tag{1}$$

The K^+ selectivity of nanopore II was confirmed by both the ratio of selectivity and the free energy profiles. Especially in the case of PMFs, a large difference in free energy was found between K^+ and Na^+ when passing through the nanopore. The mechanism of superior K^+ selectivity of graphene nanopore II was further investigated in the following section.

3.4 Mechanism of size controlled ion selectivity

Based on the study of the ion selectivity of the graphene nanopores with different sizes, nanopore II with the best ion selectivity was further investigated. As shown in Fig.7, the stable configurations of K^+ and Na^+ ions near nanopore II obtained from 10 ns MD simulations are different. From the top view of the configurations (Figs. 7a and 7b), the most stable distance of K^+ to oxygen in the nanopore is around 2.83 Å, where the K^+ ion was captured by six oxygen atoms. The lost energy due to K^+ dehydration required for K^+ to pass through the nanopore is partly compensated by its interaction with the six oxygen atoms in the nanopore. It is relatively stable for K^+ to locate in this position. The results were confirmed by the PMF in Fig.6 that this position corresponds to the saddle point of K^+ in the nanopore. Therefore, when a nanopore is of appropriate size, a balance between the electrostatic attraction and the van der Waals repulsion can be reached for an ion in the center of the nanopore (nanopore II for K^+ in this case). Due to the electrostatic attraction with O atoms, the ion can easily reach the center of the nanopore and subsequently trigger a continuous movement though the pore. However, the size of Na^+ is much smaller than that of K^+, as indicated by that the van der Waals radii given by the force field are 2.43 Å and 3.14 Å for Na^+ and K^+, respectively. As a result, the stable interaction distance of Na^+ to the O atoms of nanopore II is 2.26 Å (see Fig.7b), and finally Na^+ locates at one side of the nanopore, i.e. in the vicinity outside of the nanopore but not in the center of the nanopore. This observation is also confirmed by the RDFs of K^+/Na^+ around the O atoms in the graphene nanopore and in water as seen in Fig.7c.

The distance between K^+ and oxygen atoms in the nanopore is similar to that in water, which indicates that the center of nanopore II is a local minimum for K^+ in the PMF profile. However, the shorter distance between Na^+ ions and oxygen atoms means that a Na^+ ion is

unable to stay in the center of the nanopore. As a result, the Na^+ ion tends to move close to two of the oxygen atoms, staying away from the center of nanopore II (see Fig.7e). This is consistent with the peak position in the RDF profile of Na^+ and oxygen atoms in water (Na-OW in Fig. 7c), and also explains why the ion selectivity of nanopore I is lower than that of nanopore II.

4. Conclusion

Motivated by that ionic channels in proteins play a key role in many cellular transport phenomena we have in this work designed a series of bio-inspired graphene nanopores with different size based on a model K^+ channel protein. The analysis reveals that the ion selectivity of such graphene nanopores is controlled mostly by the size of the nanopore. It is found that doping oxygen atoms into the graphene nanopores makes them exhibit a much better K^+ to Na^+ selectivity. For the nanopore with the size of the four-oxygen ring, being 3.9 Å, Na^+ ions encountered an energy barrier of circa 21 kJ/mol higher than that for K^+ to pass through the nanopore, indicating a rate of 1000:1 in favor of K^+ to pass through, while the ion selectivity for nanopores with larger (4.2 Å) or smaller (3.2 Å) radius is clearly inferior for filtering K^+. As the radius of K^+ is larger than Na^+, and as the first peak value in the radial distribution function of the K^+ ions around the oxygen atoms is larger than for Na^+, the K^+ ions become more stable than the Na^+ ions in the nanopore with the intermediate size. The size of K^+ matches with that of the nanopore , which makes K^+ stay in the center of the nanopore, and hence makes it much easier for K^+ to pass through the nanopore than Na^+. We have thus demonstrated that

excellent ion selectivity can be obtained with biomimetic graphene nanopores and confirmed that they can be promising devices for technical applications.

Acknowledgements

The authors thank Prof. Mengbo Luo, and Dr. Peng Cui for useful discussions. This work was financially supported by the National Natural Science Foundation of China (Grant Nos. 21273200, 21003037 and 21074115), MOE (J20091551), and Zhejiang University (2011XZZX002, 2011QNA3014). The computations were performed on resources provided by the Swedish National Infrastructure for Computing (SNIC) at the parallel computer centre (PDC), through the project "Multiphysics Modeling of Molecular Materials", SNIC 020/11-23.

Author Contributions

L.J.L and Q.W. conceived the project, Q.W. provided financial support through grant application, and participated in the analysis of results, discussing and manuscript revising. Y.K, Z.S. Z, H. S, J.Q. Z, designed the experiments, and performed the research and data analyzing. H. Å, Y.Q.T participated in discussing the results. Y.K, Z.S. wrote the manuscript and L.-J.L. participated in writing the manuscript. All authors read and approved the final manuscript.

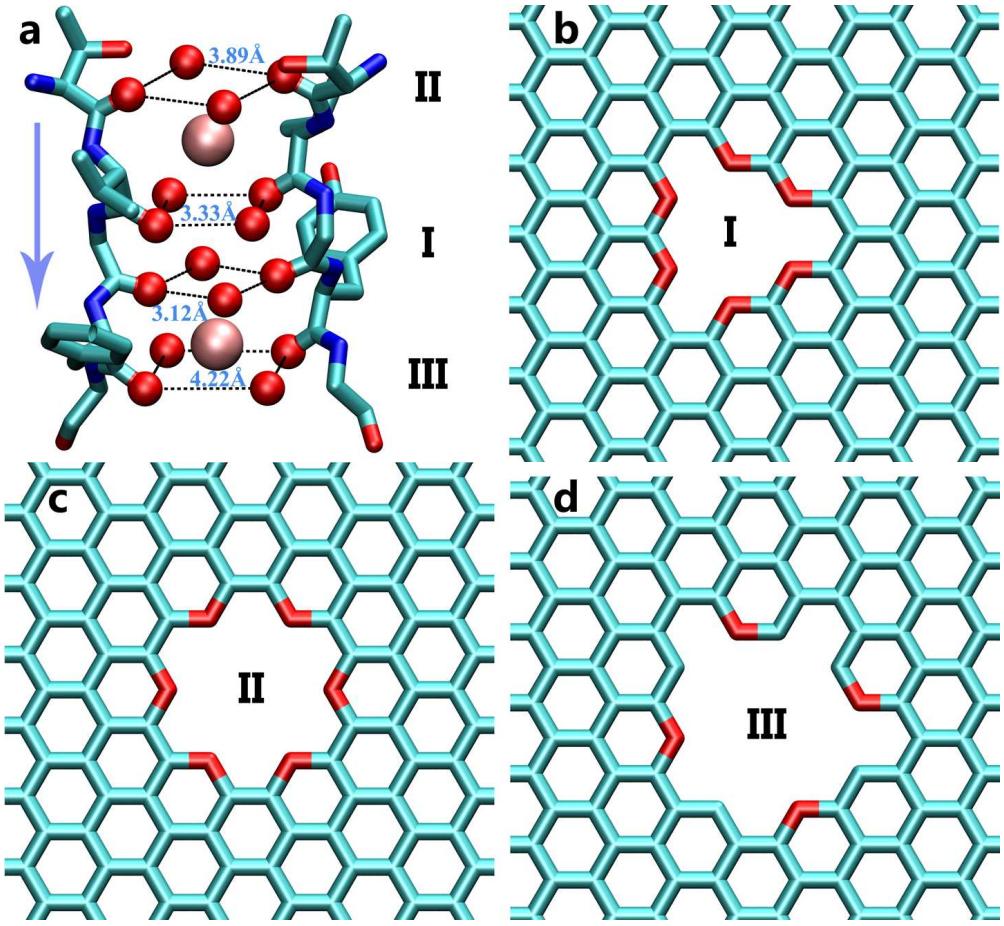

Figure 1. a) Backbone of the potassium channel of KcsA from the side view. Oxygen atoms and K^+ ions are represented as balls colored with red and pink, respectively. The light blue arrow shows the influx direction of K^+ ions. Graphene nanopores inspired from the potassium channel of KcsA, with similar distances between neighboring O atoms: b) nanopore I, with O-O distances of 3.33 Å and 3.12 Å, respectively; c) nanopore II, with O-O distance of 3.89 Å; and d) nanopore III, with O-O distance of 4.2 Å.

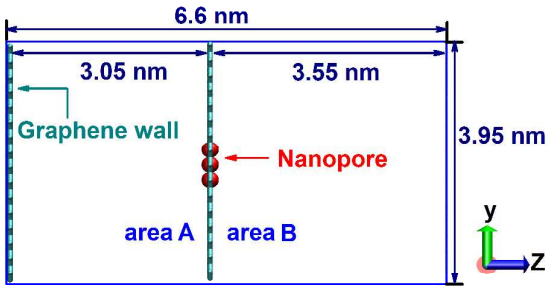

Figure 2. Side view of the grapheme sheets used in this work. An intact graphene sheet was placed at the left edge of the simulation box. A graphene sheet with a nanopore was placed in the simulation box, dividing the simulation box into two regions (denoted as "area A" and "area B" respectively).

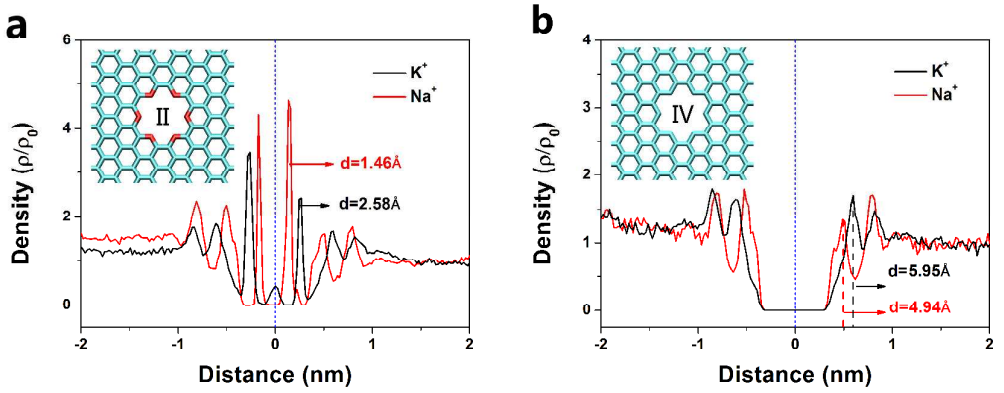

Figure 3. Density distribution of K^+/Na^+ ions in the z-axis direction of the nanopores with: a) doped with O atoms, denoted as graphene nanopore II; b) without oxygen atoms, denoted as graphene nanopore IV. The blue dashed line represents the location of the graphene nanopore.

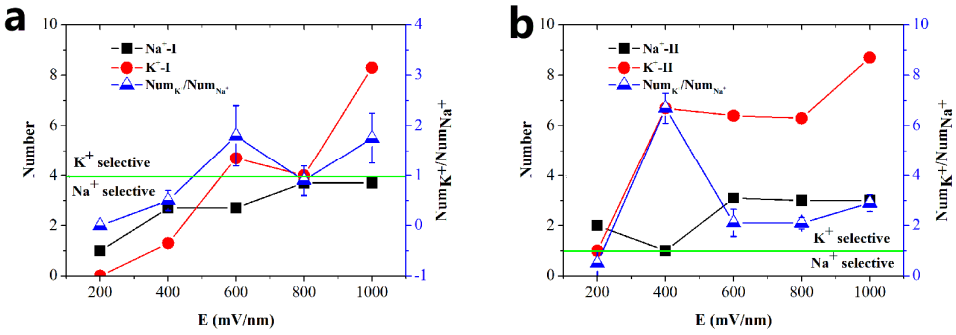

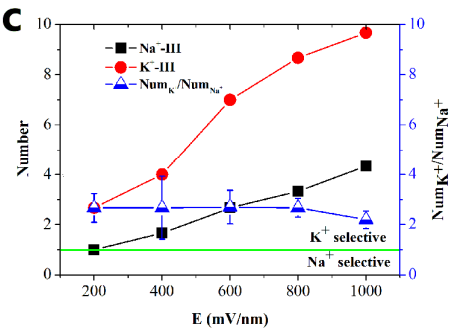

Figure 4. Number of K^+/Na^+ passing through the graphene nanopore in 10 ns MD simulations under different electric fields: a) nanopore I; b) nanopore II; c) nanopore III. Red line means the number of K^+ passing through the nanopore, black line means the number of Na^+ passing through the nanopore, and the blue line is the ratio of the number of K^+ to that of Na^+. The green line corresponds to that the ratio of the number of K^+ to that of Na^+ is 1.0.

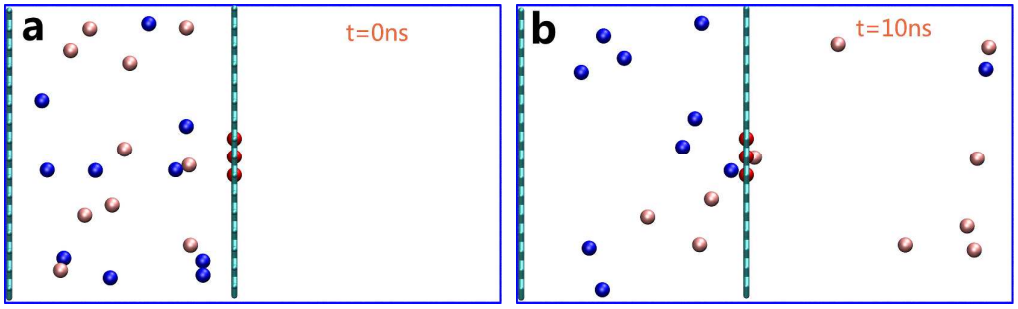

Figure 5. Snapshots taken from the MD simulation of K^+/Na^+ selectivity in nanopore II: a) t = 0 ns; b) t = 10 ns. Cl^- ions and water molecules are omitted for clarity.

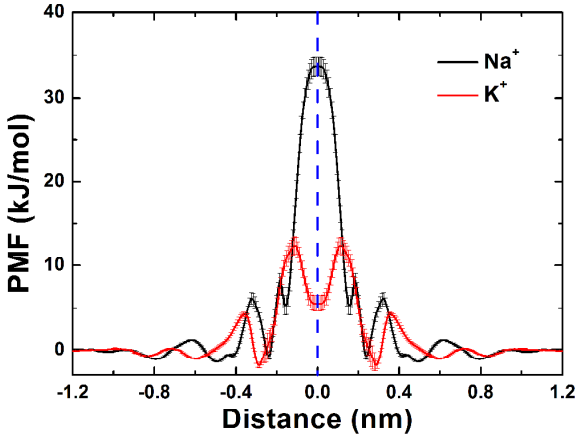

Figure 6. PMF profiles of K^+/Na^+ passing through graphene nanopore II along the reaction coordinate defined as the z-axis distance between the ions and the center of the graphene nanopore. The vertical dashed blue line represents the position of graphene nanopore II.

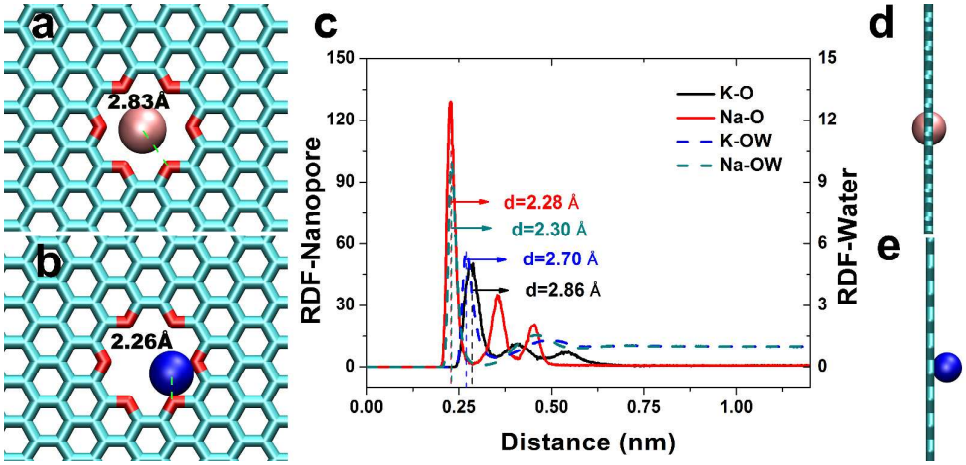

Figure 7. Stable configuration of K^+ (pink) and Na^+ (blue) near nanopore II: (a) and (b) from the top view; (d) and (e) from the side view. (c) The RDFs of K^+/Na^+ around the O atoms in nanopore II and RDFs of O atoms in water around K^+/Na^+.

References

1. M. J. Ackerman and D. E. Clapham, *New England Journal of Medicine*, 1997, 336, 1575-1586.
2. Y. Zhou, J. H. Morais-Cabral, A. Kaufman and R. MacKinnon, *Nature*, 2001, 414, 43-48.
3. W. A. Catterall, *Science*, 1988, 242, 50-61.
4. X. Gong, J. Li, K. Xu, J. Wang and H. Yang, *J. Am. Chem. Soc.*, 2010, 132, 1873-1877.
5. M. Kumar, M. Grzelakowski, J. Zilles, M. Clark and W. Meier, *Proc. Natl. Acad. Sci. U.S.A.*, 2007, 104, 20719-20724.
6. E. T. Lam, A. Hastie, C. Lin, D. Ehrlich, S. K. Das, M. D. Austin, P. Deshpande, H. Cao, N. Nagarajan, M. Xiao and P.-Y. Kwok, *Nat. Biotech.*, 2012, 30, 771-776.
7. S. Liu, Q. Pu, L. Gao, C. Korzeniewski and C. Matzke, *Nano Lett*, 2005, 5, 1389-1393.
8. C. H. Nielsen, *Anal. Bioanal. Chem.*, 2009, 395, 697-718.
9. J. D. Neely, M. Amiry-Moghaddam, O. P. Ottersen, S. C. Froehner, P. Agre and M. E. Adams, *Proc. Natl. Acad. Sci. U.S.A.*, 2001, 98, 14108-14113.
10. M. Zhang, X. Hou, J. Wang, Y. Tian, X. Fan, J. Zhai and L. Jiang, *Adv. Mater.*, 2012, 24, 2424-2428.
11. D. A. Puleo, R. A. Kissling and M. S. Sheu, *Biomaterials*, 2002, 23, 2079-2087.
12. C. Sathe, X. Q. Zou, J. P. Leburton and K. Schulten, *Acs Nano*, 2011, 5, 8842-8851.
13. C. A. Merchant, K. Healy, M. Wanunu, V. Ray, N. Peterman, J. Bartel, M. D. Fischbein, K. Venta, Z. T. Luo, A. T. C. Johnson and M. Drndic, *Nano Lett*, 2010, 10, 2915-2921.
14. C. A. Merchant and M. Drndic, *Methods Mol Biol*, 2012, 870, 211-226.
15. A. K. Geim, *Science*, 2009, 324, 1530-1534.
16. A. K. Geim and K. S. Novoselov, *Nat. Mater.*, 2007, 6, 183-191.
17. F. Banhart, J. Kotakoski and A. V. Krasheninnikov, *Acs Nano*, 2010, 5, 26-41.
18. A. Du, Z. Zhu and S. C. Smith, *J. Am. Chem. Soc.*, 2010, 132, 2876-2877.
19. S. Garaj, W. Hubbard, A. Reina, J. Kong, D. Branton and J. A. Golovchenko, *Nature*, 2010, 467, 190-U173.
20. D.-e. Jiang, V. R. Cooper and S. Dai, *Nano Lett*, 2009, 9, 4019-4024.
21. L. Liang, P. Cui, Q. Wang, T. Wu, H. Agren and Y. Tu, *RSC Advances*, 2013, 3, 2445-2453.
22. D. B. Wells, M. Belkin, J. Comer and A. Aksimentiev, *Nano Lett*, 2012, 12, 4117-4123.
23. A. Aksimentiev, *Nanoscale*, 2010, 2, 468-483.
24. K. Sint, B. Wang and P. Král, *J. Am. Chem. Soc.*, 2008, 130, 16448-16449.
25. C. Zhu, H. Li, X. C. Zeng, E. Wang and S. Meng, *Scientific Reports*, 2013, 3, 3163.
26. D. A. Doyle, J. M. Cabral, R. A. Pfuetzner, A. Kuo, J. M. Gulbis, S. L. Cohen, B. T. Chait and R. MacKinnon, *Science*, 1998, 280, 69-77.

27. E. Jordan, R. G. Bell, D. Wilmer and H. Koller, *J. Am. Chem. Soc.*, 2006, 128, 558-567.
28. M. C. Duke, J. C. D. Da Costa, D. D. Do, P. G. Gray and G. Q. Lu, *Adv. Funct. Mater.*, 2006, 16, 1215-1220.
29. I. Kim and T. W. Allen, *Proc. Natl. Acad. Sci. U.S.A.*, 2011, 108, 17963-17968.
30. G. Kresse and J. Furthmüller, *Phys. Rev. B*, 1996, 54, 11169-11186.
31. G. Kresse and J. Hafner, *Phys. Rev. B*, 1993, 47, 558-561.
32. J. P. Perdew, K. Burke and M. Ernzerhof, *Phys. Rev. Lett.*, 1996, 77, 3865-3868.
33. H. J. Monkhorst and J. D. Pack, *Phys. Rev. B*, 1976, 13, 5188-5192.
34. D. Van Der Spoel, E. Lindahl, B. Hess, G. Groenhof, A. E. Mark and H. J. C. Berendsen, *J. Comput. Chem.*, 2005, 26, 1701-1718.
35. D. Van Der Spoel, E. Lindahl, B. Hess, A. R. van Buuren, E. Apol, P. J. Meulenhoff, D. P. Tieleman, A. L. T. M. Sijbers, K. A. Feenstra, R. van Drunen and H. J. C. Berendsen, *Gromacs User Manual version 4.5*, 2010, DOI: 10.1073/pnas.1012276108/-/DCSupplemental.
36. W. Humphrey, A. Dalke and K. Schulten, *J. Mol. Graphics*, 1996, 14, 33-38.
37. W. L. Jorgensen, J. Chandrasekhar, J. D. Madura, R. W. Impey and M. L. Klein, *J. Chem. Phys.*, 1983, 79, 926-935.
38. A. D. MacKerell, D. Bashford, Bellott, R. L. Dunbrack, J. D. Evanseck, M. J. Field, S. Fischer, J. Gao, H. Guo, S. Ha, D. Joseph-McCarthy, L. Kuchnir, K. Kuczera, F. T. K. Lau, C. Mattos, S. Michnick, T. Ngo, D. T. Nguyen, B. Prodhom, W. E. Reiher, B. Roux, M. Schlenkrich, J. C. Smith, R. Stote, J. Straub, M. Watanabe, J. Wiórkiewicz-Kuczera, D. Yin and M. Karplus, *J. Chem. Phys. B*, 1998, 102, 3586-3616.
39. L.-J. Liang, Q. Wang, T. Wu, T.-Y. Sun and Y. Kang, *ChemPhysChem*, 2013, 14, 2902-2909.
40. L.-J. Liang, T. Wu, Y. Kang and Q. Wang, *ChemPhysChem*, 2013, 14, 1626-1632.
41. T. Darden, D. York and L. Pedersen, *J. Chem. Phys.*, 1993, 98, 10089-10092.
42. J. O. Hirschfelder, C. F. Curtiss and R. B. Bird, John Wiley and Sons, New York, 1954.
43. B. Roux, *Comput. Phys. Commun.*, 1995, 91, 275-282.
44. M. Souaille and B. t. Roux, *Comput. Phys. Commun.*, 2001, 135, 40-57.
45. G. M. Torrie and J. P. Valleau, *Chem. Phys. Lett.*, 1974, 28, 578-581.
46. S. Kumar, J. M. Rosenberg, D. Bouzida, R. H. Swendsen and P. A. Kollman, *J. Comput. Chem.*, 1992, 13, 1011-1021.
47. Z. He, J. Zhou, X. Lu and B. Corry, *Acs Nano*, 2013, 7, 10148-10157.